HHS Public Access

Author manuscript

Biomed Mater. Author manuscript; available in PMC 2019 May 02.

Published in final edited form as:

Biomed Mater. ; 13(4): 045009. doi:10.1088/1748-605X/aabb31.

The Effects of Hydroxyapatite Nanoparticles Embedded in a MMP-sensitive Photoclickable PEG Hydrogel on Encapsulated MC3T3-E1 Pre-Osteoblasts

Maria Carles-Carner[a], **Leila S. Saleh**, and **Stephanie J. Bryant**[a,b,c]

[a]Department of Chemical and Biological Engineering, University of Colorado, 3415 Colorado Avenue, Boulder, CO 80303, USA

[b]BioFrontiers Institute, University of Colorado, 3415 Colorado Avenue, Boulder, CO 80303, USA

[c]Material Science and Engineering Program, University of Colorado, 3415 Colorado Avenue, Boulder, CO 80303, USA

Abstract

This study investigated the effects of introducing hydroxyapatite nanoparticles into a matrix metalloproteinase (MMP) sensitive poly(ethylene glycol) (PEG) hydrogel containing cell adhesion peptides of RGD for bone tissue engineering. MC3T3-E1 pre-osteoblasts were encapsulated in the biomimetic PEG hydrogel, which was formed from the photoclick thiol-norbornene reaction system, cultured for up to 28 days in growth medium or osteogenic differentiation medium, and evaluated by cellular morphology and differentiation by alkaline phosphatase activity and bone-like extracellular matrix (ECM) deposition for mineral and collagen. Hydroxyapatite nanoparticles were incorporated during hydrogel formation and cell encapsulation at 0, 0.1 or 1% (w/w). Incorporation of hydroxyapatite nanoparticles did not affect the hydrogel properties as measured by compressive modulus and equilibrium swelling. In growth medium, encapsulated MC3T3-E1 cells remained largely round regardless of hydroxyapatite concentration. Alkaline phosphatase activity increased by 25% at day 14 and total collagen content increased by 55% at day 28 with increasing hydroxyapatite concentration from 0 to 1%. In differentiation medium, cell spreading was evident regardless of hydroxyapatite indicating that the MC3T3-E1cells were able to degrade the hydrogel. For the 1% hydroxyapatite condition, alkaline phosphatase activity was 27% higher at day 14 and total collagen content was 22% higher at day 28 in differentiation medium when compared to growth medium. Mineral deposits were more abundant and spatial elaboration of collagen type I was more evident in the 1% (w/w) hydroxyapatite condition with differentiation medium when compared to all other conditions. Overall, osteogenesis was observed in the hydrogels with hydroxyapatite nanoparticles in growth medium but was enhanced in differentiation medium. In summary, a biomimetic hydrogel comprised of MMP-sensitive crosslinks, RGD cell adhesion peptides, and 1% (w/w) hydroxyapatite nanoparticles is promising for bone tissue engineering.

Correspondence to: Stephanie J. Bryant.

1. Introduction

In situ forming hydrogels are promising platforms to deliver cells through minimally invasive methods and in a three-dimensional (3D) environment for tissue engineering [1–3]. The former enables filling irregularly shaped defects without *a priori* knowledge. The latter offers the opportunity to create environments that help guide cells and create neotissue. Synthetic hydrogels are promising for their reproducible properties (e.g., mechanical and swelling) and tunable rates of degradation both of which can affect the cells and their ability to synthesize neotissue [4]. Since cells do not directly interact with synthetic polymers, extracellular matrix (ECM) moieties have been introduced with precision to create biomimetic hydrogels that emulate aspects of the native ECM and which can be tailored to a particular cell type [5–8]. In addition, peptide crosslinks that are sensitive to cell secreted enzymes have been introduced into synthetic hydrogels to create hydrogels whose degradation is mediated by cell-secreted enzymes [9,10]. Collectively, synthetic hydrogels offer many of the biological benefits of natural hydrogels, but with greater control and tunablity.

One promising synthetic hydrogel, which has been investigated for cell encapsulation and bone tissue engineering, is poly(ethylene glycol) (PEG) hydrogels [11]. Cell adhesion peptides have been introduced into PEG hydrogels, such as RGD and RRETAWA, which are recognized by the integrin α5β1 [12,13] that is important in osteogenesis [14]. PEG hydrogels with RGD have been shown to improve viability of encapsulated mesenchymal stem cells and enhance osteogenesis and facilitate greater mineralization when compared to hydrogels without the peptide [15,16]. Studies have also encapsulated stem cells in matrix metalloproteinase (MMP)-sensitive hydrogels and demonstrated osteogenesis by increased alkaline phosphatase activity with culture time and the presence mineral deposits [17]. However, *in vivo* studies in bone defects of animal models report that simply incorporating adhesion peptides and MMP-sensitive crosslinks into a hydrogel such as PEG hydrogels is insufficient to promote bone ingrowth [18,19]. Osteoinductive factors, like bone morphogenetic factor 2, are needed to induce bone ingrowth *in vivo* [18,19]. Collectively, these and other studies support the idea that incorporating ECM analogs and degradation moieties into a PEG hydrogel supports osteogenesis capabilities, but that osteoinductive factors will be necessary when translating to *in vivo* conditions.

One simple approach to create an osteoinductive environment is through the incorporation of hydroxyapatite particles into a hydrogel [20–24]. Studies have shown that introducing hydroxyapatite particles into a hydrogel enhances osteogenesis of mesenchymal stem cells when cells are seeded on top of [25] or encapsulated in [26] hydrogels containing hydroxyapatite particles. Hydroxyapatite particles have been encapsulated in PEG hydrogels to control protein release for drug delivery applications [27], improve the mechanical properties [28,29], and serve as a nucleation site for further mineralization [21]. The latter can be particularly important as adding in high amounts of mineral (e.g., bone is ~60–70% mineral) in a hydrogel setting is challenging [30].

The overall objective of this study was to incorporate hydroxyapatite nanoparticles into a PEG hydrogel containing the cell adhesion peptide, RGD, and MMP-sensitive crosslinks to

create a bone-mimetic biodegradable hydrogel for potential use in bone tissue engineering. PEG hydrogels formed from the photoclick thiol:norbornene reaction were chosen for its ease and promise in tissue engineering [31,32]. This study investigated the effect of hydroxyapatite nanoparticle concentration on osteogenic differentiation and bone-like ECM deposition by MC3T3-E1 pre-osteoblastic cells that were encapsulated in the biomimetic PEG hydrogel and cultured *in vitro*. The response of MC3T3-E1 cells was investigated as a function of hydroxyapatite nanoparticle concentrations (0%, 0.1% and 1% w/w) without and with osteogenic factors (*i.e.,* growth medium and osteogenic medium, respectively) over the course of 28 days. A low concentration of hydroxyapatite nanoparticles was chosen to investigate the osteogenic capabilities of the nanoparticles without altering the hydrogel properties. Collectively findings from this study show that introducing hydroxyapatite nanoparticles improves the osteogenic response of MC3T3-E1 cells in the absence of differentiation factors and further improves the osteogenic capabilities with differentiation factors.

2. Materials and Methods

2.1 Macromer Synthesis and Hydrogel Formation

The 8-arm poly(ethylene glycol)-norbornene (8-arm-PEG-NB) macromolecular monomer was synthesized from 8-arm PEG-NH_2 (20kDa, JenKem USA) as previously described [32]. Functionalization was determined by ^{1}H NMR to be ~100% (i.e., each arm of the multi-arm PEG macromolecular monomer was functionalized with a norbornene). Hydroxyapatite nanoparticles were purchased (size range <200 nm per manufacturer, Sigma) and sterilized by autoclave. Sterile hydroxyapatite nanoparticles were suspended in phosphate buffer saline (PBS, Cellgro), sonicated for 20 min. A hydrogel precursor solution was prepared to achieve a final concentration of 8% (w/w) 8-arm-PEG-NB, MMP-2 sensitive peptide crosslinker (CVPLSLYSGC, GenScript) at a 0.83 thiol:ene ratio, 2.5 mM of cell adhesion peptide (CRGDS, GenScript), 0.05% (w/w) of photoinitiator (Irgacure 2959, BASF), which was sterile filtered (0.22μm). The precursor solution was then combined with a sterile hydroxyapatite nanoparticle solution to a final concentration of 0, 0.1, or 1% (w/w) hydroxyapatite. Hydrogel disks of 4.5 mm diameter and 2 mm height were made in cylindrical molds by polymerizing the hydrogel precursor solution under 352 nm light at 6 mW/cm^2 for ~6–7 minutes.

2.2 Hydrogel Characterization

Acellular hydrogels were swollen to equilibrium in PBS for 24 hours. Equilibrium swollen hydrogels were subjected to unconfined compression (MTS Synergie 100) at a constant strain rate (0.5 mm/min). The tangent modulus was determined in the linear range between 10 and 15% strain and reported as the compressive modulus. Equilibrium swollen hydrogels were weighed (wet weight, m_w) and then lyophilized to obtain polymer dry weight (m_d). The mass swelling ratio was determined by m_w/m_d. Morphology and size of the hydroxyapatite nanoparticles were characterized by field emission scanning electron microscopy (SEM, JEOL JSM-7401F) using a gold sputtered coating. Particle size was estimated from SEM images using NIH Image J. Bright field images were also acquired of hydrogels to assess the distribution of the nanoparticles.

2.3 MC3T3-E1 Cell Encapsulation

The murine pre-osteoblast-like cell line MC3T3-E1 (ATCC, CRL-2593) was used. The cells have the capacity to differentiate into osteoblasts and have been demonstrated to deposit mineral *in vitro* [33]. MC3T3-E1 cells were expanded in growth media (Minimum Essential Medium, α-MEM (Gibco) supplemented with 10% of fetal bovine serum (FBS, Atlanta Biologicals) and 1% antibiotics (5,000 Units/mL Penicillin, 5,000 μg/mL Streptomycin, Corning) in a humidified atmosphere at 37°C and 5% CO_2. Cells were passaged at ~80–90% confluency with 0.25% Trypsin-EDTA (Gibco). MC3T3-E1 cells were combined with the hydrogel precursor solution at 20×10^6 cells/ml and the hydrogel was formed as described above. The cell-laden hydrogels were cultured in osteogenic differentiation media comprised of growth media supplemented with 10 mM β-glycerophosphate (Sigma, St. Louis, MO), 50 mM L-Ascorbic acid 2-phosphate sesquimagnesium salt hydrate (Sigma) and 0.1 mM Dexamethasone (Sigma). A separate set of hydrogels without cells were formed and cultured in osteogenic differentiation medium for 28 days. All procedures were performed inside a biosafety cabinet using previously sterilized instruments.

2.4 Raman Spectroscopy

Samples were analyzed by Raman spectroscopy. Acellular hydrogels containing 0, 0.1, or 1% (w/w) hydroxyapatite nanoparticles were lyophilized and then imaged. For MC3T3-E1 cell-laden hydrogels, the samples were prepared for histology (described below), sectioned, and stained for von Kossa and then imaged. Raman spectra were collected using a Horiba LabRAM HR Evolution Raman spectrometer at the Raman Microspectroscopy Laboratory, University of Colorado at Boulder. The 532nm (green) laser beam was focused through a 50x LWD (0.75 NA) objective lens, yielding a spatial resolution of ~2 μm and power at the sample surface of 29 mW. A 600 lines/mm grating and a 100 μm confocal pinhole were used to give a spectral resolution of 4.5 cm^{-1} full width at half maximum. The spectrometer was calibrated using the 520 cm^{-1} Raman peak of Si prior to analysis. Spectra were collected by averaging 15 accumulated spectra collected with a 2 sec counting time. Spectral data were corrected for instrumental artifacts and a polynomial baseline was subtracted in LabSpec 6 (Horiba Scientific).

2.5 Viability, Biochemical Assays, and Mechanical Tests

At select time points (initial (24 hours post-encapsulation), 14 and 28), hydrogels were removed from culture. One set of hydrogels was analyzed for viability and cell morphology by Live/Dead Cell Viability Assay staining kit (Life Technologies, Thermo Fisher Scientific), which uses Calcein-AM to stain live cells green and ethidium homodimer to stain dead cells red. A second set of hydrogels was transferred DNAse free water and disrupted with a tissue lyser (Qiagen). Hydrogel lysates were assessed for total DNA content with the Quant-iT PicoGreen dsDNA Assay Kit (Thermo Fisher Scientific) and measured at an excitation of 485 nm and emission of 520 nm, alkaline phosphatase activity by enzyme cleavage of p-nitrophenol phosphate and measuring absorbance at 450 nm and total collagen content by digesting the samples with pepsin powder (Worthington) in 0.5M acetic acid overnight and incubated with Sirius Red (Sigma) and measuring absorbance at 544 nm. All assays were performed following the instructions and protocols provided by the

manufacturer's and using a spectrophotometer. The compressive modulus of cellular hydrogels was measured as described for acellular hydrogels.

2.6 (Immuno)histochemistry

For immunohistochemical and histological analysis the hydrogels were collected initially at 24 hours post-encapsulation and at day 28 and fixed in neutral-buffered formalin for 30 minutes at room temperature inside the fumes hood. Hydrogels were dehydrated and embedded in paraffin wax. The samples were sectioned in 10 μm slices and processed for histological staining. Sections were stained for mineral by von Kossa stain following standard protocol using 1% (w/w) silver nitrate (Sigma) under ultraviolet light for 30 minutes. Sections were counter stained with nuclear fast red (RICCA Chemical Company). Mineral stains black and nuclei stain pink to red. Acellular hydrogels cultured in differentiation medium for 28 days were sectioned and stained by von Kossa for mineral deposits. Sections were imaged using light microscopy (Axiovert 40 C Zeiss). A separate set of sections from the cellular hydrogels were pretreated with 1 mg/mL pepsin (Sigma), subjected to antigen retrieval (Retrievagen, BD Biosciences), permeabilized, and blocked. Sections were then incubated with collagen I antibody (1:50, Abcam, ab34710) in blocking solution overnight at 4°C and then treated with a secondary antibody, AlexaFluor 546 goat anti-rabbit antibody (1:200, Invitrogen), for one hour at room temperature. Nuclei were counterstained with 4′,6-diamidino-2-phenylindole (DAPI). Sections were imaged by laser scanning confocal microscopy (Zeiss LSM5 Pascal).

2.7 Statistical Analysis

Data are presented as the mean of n=3 replicates with standard deviation parenthetically in the text or as error bars in the figures. Statistical analysis was performed using Real Statistics add-in for Excel. Acellular hydrogel data were analyzed by a one-way ANOVA with hydroxyapatite concentration as the factor. Cellular hydrogel data were analyzed by a three-way ANOVA. Factors were culture time, hydroxyapatite concentration (% (w/w)) and culture medium (growth medium or osteogenic differentiation medium). If the three-way interaction was statistically significant, follow up tests were performed and included simple two-way interactions and simple main effects. Post-hoc analysis was performed Tukey's HSD with $\alpha=0.05$. A p-value of <0.05 was used to determine statistical significance.

3. Results

3.1 Characterization of Acellular Hydrogels

Biomimetic PEG hydrogels were fabricated with cell adhesion peptides of RGD, MMP-sensitive crosslinkers and entrapped hydroxyapatite nanoparticles (figure 1). The concentration of hydroxyapatite nanoparticles ranged from 0 to 0.1 to 1% (w/w). The hydrogels were initially characterized in the absence of cells (figure 2). The compressive modulus of the hydrogels was 41 (5) kPa without hydroxyapatite particles and was not affected by the incorporation of hydroxyapatite particles (figure 2(a)). Similarly, the mass swelling ratio of the hydrogels was 18 (3) without hydroxyapatite particles and was not affected by the incorporation of hydroxyapatite particles (figure 2(b)). Confirmation of hydroxyapatite particles on whole gel specimen was determined by Raman spectroscopy

(figure 2(c)). The characteristic peak associated with hydroxyapatite at 960 cm^{-1}, which represents the calcium phosphate group in hydroxyapatite, was present in the hydrogels with hydroxyapatite nanoparticles, but was not apparent in the PEG hydrogel lacking hydroxyapatite. The morphology of the hydroxyapatite nanoparticles by SEM indicated a round morphology with an average size of 100 (25) nm (figure 2(d)). The nanoparticles were distributed throughout the hydrogel as indicated by bright field images of whole gel samples.

3.2 MC3T3-E1 Viability, Morphology, and Number in Hydrogels

Representative confocal microscopy images assessing viability and morphology of encapsulated MC3T3-E1 cells as a function of hydroxyapatite nanoparticle concentration, culture time and culture medium are shown in figure 3(a). Qualitatively, viable MC3T3-E1 cells were present throughout the experiment and across all experimental groups. Initially (i.e., 24 hours post-encapsulation), the encapsulated MC3T3-E1 cells displayed a round morphology. There was evidence of a few cells spreading by day 14, which was maintained at day 28 in growth media across all hydroxyapatite nanoparticle concentrations. However, when cultured in differentiation media, cell spreading was more pronounced by day 14 and even greater by day 28 with the apparent formation of intercellular connections. There was no apparent difference in morphology as a function of hydroxyapatite concentration within each media experimental group. The apparent over exposure in the confocal microscopy images at day 28 is attributed to an increase in collagen deposition surrounding the cells, which made imaging more difficult.

The total number of cells within the hydrogels in each experimental group was assessed quantitatively by dsDNA content (figure 3(b)). A three-way ANOVA was run to examine the effect of time, hydroxyapatite nanoparticle concentration and culture medium. There was not a significant three-way interaction nor were the two-way interactions among the factors significant. Time was the only factor that had a significant effect ($p<0.001$) on dsDNA content. The amount of dsDNA significantly decreased from the initial time point for the 0% hydroxyapatite condition at day 14 in growth and differentiation media and for the 1% hydroxyapatite condition in growth medium at day 28 and in differentiation medium at days 14 and 28. The largest decrease was ~30% from the initial time point, which was observed in the 1% hydroxyapatite condition in differentiation medium.

3.3 Alkaline Phosphatase and Mineralization

Alkaline phosphatase (ALP) activity was assessed as a measure osteoblast differentiation as a function of culture time, hydroxyapatite nanoparticle concentration, and culture medium (figure 4(a)). A three-way ANOVA was run to examine the effect of time, hydroxyapatite concentration and culture medium. There was not a significant three-way interaction. There was a significant two-way interaction ($p=0.034$) between time and hydroxyapatite nanoparticle concentration, but not among the other factors. Culture medium had a significant effect ($p=0.002$) on ALP activity. Follow-up analyses were performed to determine the simple effects for time and hydroxyapatite concentration. At day 14, ALP activity was highest for the 1% (w/w) hydroxyapatite nanoparticle condition within each culture medium experimental group compared to the 0 and 0.1% (w/w) hydroxyapatite nanoparticle condition. In addition, ALP activity was higher for the differentiation medium

condition compared to the growth medium condition at day 14. At day 28, differences in ALP activity were not significant among the different experimental groups.

The hydrogels were stained for mineral deposits by von Kossa initially and after 28 days of culture (figure 4(b)). Qualitatively, there was minimal positive staining initially in the hydrogels without hydroxyapatite nanoparticles. There was faint staining for mineral in the hydrogels containing hydroxyapatite nanoparticles. In growth medium after 28 days, there was evidence of punctate mineral deposits across all experimental groups. Mineral deposition appeared to increase with increasing hydroxyapatite nanoparticle concentration. In differentiation medium, there was some evidence of punctate mineral deposits in the hydrogel without hydroxyapatite nanoparticles. Punctate mineral deposits were more pronounced in the 0.1% (w/w) hydroxyapatite experimental group. However, in the 1% (w/w) hydroxyapatite experiment group, mineral deposition was present throughout the hydrogel construct. In hydrogels cultured in differentiation medium, but without cells, minimal staining for mineral was evident with no hydroxyapatite nanoparticles at day 28. Acellular hydrogels with 0.1% (w/w) hydroxyapatite showed punctate mineral deposits at day 28. However, at day 28, acellular hydrogels with 1% (w/w) hydroxyapatite exhibited mineral deposits throughout the hydrogel, similar to the cellular constructs at day 28. Overall, mineral deposition was more pronounced in the hydrogels containing hydroxyapatite nanoparticles when cultured in differentiation medium compared to growth medium and was similar regardless of the presence of cells.

Raman spectra were collected for all cellular experimental groups at day 28 (figure 4(c)). The regions that stained positive for mineral by von Kossa were evaluated by Raman spectroscopy. All experimental groups indicated the presence of the hydroxyapatite at 960 cm^{-1}.

3.4 Collagen Accumulation in Cellular Hydrogels

Total collagen content normalized to dsDNA was assessed as a function of culture time, hydroxyapatite nanoparticle concentration, and culture medium (figure 5(a)). A three-way ANOVA was run to examine the effect of time, hydroxyapatite nanoparticle concentration and culture medium. There was not a significant three-way interaction. There was a significant two-way interaction between time and hydroxyapatite concentration ($p<0.001$) and between time and culture medium ($p=0.019$), but not between hydroxyapatite concentration and culture medium. Follow-up experiments were performed to determine the simple effects for time, hydroxyapatite concentration, and culture medium. Collagen content significantly increased with culture time within each hydroxyapatite nanoparticle concentration and culture medium experimental group. The 1% (w/w) hydroxyapatite nanoparticle concentration had the highest collagen content at day 28 within each culture medium experimental group. At day 28, collagen content was significantly higher in the differentiation medium condition for the 0.1% and 1% hydroxyapatite nanoparticle concentrations when compared to the growth medium condition.

The spatial distribution of collagen type I was also assessed by immunohistochemistry (figure 5(b)). There was no detectable collagen I staining initially in hydrogels without hydroxyapatite. However, with 1% (w/w) hydroxyapatite, pericellular deposition of collagen

type I was evident at the initial time point (i.e., 24 hours post-encapsulation). By day 28 in growth medium and differentiation medium, collagen type I was present in all experimental groups. The spatial deposition of collagen type I appeared to be most abundant in the experimental group with 1% (w/w) hydroxyapatite nanoparticle concentration and differentiation medium.

3.5 Mechanical Properties of Cell-Laden Hydrogels

The compressive modulus of the cellular constructs was assessed as a function of culture time, hydroxyapatite nanoparticle concentration, and culture medium (figure 6). The modulus initially was ~25 kPa regardless of hydroxyapatite nanoparticle concentration. A three-way ANOVA was run to examine the effect of time, hydroxyapatite nanoparticle concentration and culture medium. There was a significant three-way interaction ($p < 0.001$). In follow-up tests, two-way ANOVAs were run. There were no significant two-way interactions. For time and hydroxyapatite nanoparticle concentration in growth medium, time was a factor ($p=0.034$), but not hydroxyapatite concentration. There was a 20% drop ($p=0.014$) in the compressive modulus from the initial time point to day 14 for the 1% hydroxyapatite experimental group in growth medium, but by day 28 the modulus was not significantly different. There were no other significant main effects on the compressive modulus. Overall and throughout the course of the culture, there were minimal changes in the compressive modulus.

4. Discussion

This study demonstrates that the incorporation of hydroxyapatite nanoparticles into a MMP-sensitive PEG hydrogel with RGD enhances cell spreading and differentiation of MC3T3-E1 pre-osteoblast cells. Alkaline phosphatase activity, mineral deposits and collagen content were elevated with increasing amounts of incorporated hydroxyapatite. While hydroxyapatite on its own induced osteogenesis within these hydrogels, differentiation cues in the culture medium combined with the highest hydroxyapatite concentration at 1% (w/w) had the most significant positive effect on osteogenesis of encapsulated MC3T3-E1 cells.

The interaction between cells and their surrounding matrix, via adhesion ligands, influences the differentiation fate [34,35]. While studies have reported that cell spreading is critical to osteogenesis, others have reported that the degree of cell-matrix interactions in the absence of cell spreading is important to osteogenesis [36,37]. In the absence of incorporated hydroxyapatite nanoparticles, the MC3T3-E1 cells appeared to maintain a largely rounded morphology throughout the 28 days of culture in growth medium without differentiation cues. Nonetheless, osteogenic differentiation was evident by increased alkaline phosphatase activity and mineral deposits that were positive for hydroxyapatite. On the contrary, in the presence of soluble differentiation cues, the MC3T3-E1 cells locally degraded the hydrogel enabling extension of their cellular processes and cell spreading, which was evident by fourteen days. In this experimental group, osteogenesis was improved over growth medium. MMPs, including MMP-2, have been shown to be upregulated during osteogenesis [38,39]. These observations suggest that cues in the differentiation medium may have led to higher MMP activity concomitant with enhanced osteogenic differentiation [39]. It remains to be

determined whether cell spreading contributed to the enhanced osteogenesis of the MC3T3-E1 cells or whether the differentiation cues in the media were the predominant factor and that led to the enhanced osteogenesis. It has been suggested that osteoblasts may adopt different cellular morphologies depending on their environment to achieve a similar internal stress state to support their phenotype [40]. Thus, it is possible that different morphologies, such as those observed in this study and other studies [36,37], may support osteogenesis. Although cell spreading was not evident in the growth medium, it is possible that cells may have extended processes that resemble smaller dendrite-like processes [40], which are more difficult to detect. Additional studies are needed to better understand the connection between osteogenesis, cell-mediated degradation of the hydrogel, and cell morphology in these MMP-sensitive PEG hydrogels.

The incorporation of hydroxyapatite nanoparticles (0.1 or 1% w/w) had significantly positive effects on osteogenesis of encapsulated MC3T3-E1 pre-osteoblast cells. The mechanism by which hydroxyapatite is osteoinductive is not completely understood. It has been suggested that cell adhesion to hydroxyapatite surfaces via non-specific protein adsorption is one mechanism that induces osteogenesis [41,42]. In addition, studies have shown that the osteogenic growth factors (e.g., bone morphogenetic protein (BMP)) readily adsorb to hydroxyapatite surfaces which enhances osteogenesis [43]. Indirect cultures with hydroxyapatite nanoparticles have also shown enhanced osteogenesis [44]. This indirect mechanism has been attributed to changes in the local concentration of calcium and phosphate ions [44,45], which can affect intracellular signaling and subsequently may influence differentiation [44,46]. In this study, it is possible that MC3T3-E1 cells interact directly and/or indirectly with the hydroxyapatite nanoparticles. The mesh size of the swollen hydrogel is estimated to be ~50 nm [47], suggesting that the majority of the nanoparticles, estimated to be ~100 nm, will be entrapped in the hydrogel network. However, the release of hydroxyapatite nanoparticles was not assessed. Cells may, therefore, interact directly with the nanoparticles in solution prior to encapsulation or as the cells locally degrade the hydrogel where they can come into contact with the entrapped nanoparticles. The low volume fraction of the nanoparticles (~0.03 or 0.3% v/v) made it difficult to identify them initially in the histological sections through the von Kossa stain, thus it was not possible to determine if they were associated with cells or not. Cells may also interact indirectly with the hydroxyapatite particles possibly through changes in the local ion concentration or through sequestration of proteins and/or growth factors from the culture medium and/or from MC3T3-E1 cells themselves. As cells undergo osteogenesis they will secrete their own BMPs leading to autocrine and paracrine effects that help to support differentiation [48]. Regardless of the osteoinductive nature of the hydroxyapatite nanoparticles in the hydrogels, a positive effect on osteogenesis was evident and was more pronounced with increasing hydroxyapatite concentrations.

An ECM comprised of mineral deposits and collagen, specifically collagen type I, was enhanced in the MMP-sensitive PEG hydrogels with incorporated hydroxyapatite nanoparticles in growth medium. Interestingly, hydroxyapatite deposits were detected even in the experimental group without the incorporation of the nanoparticles in growth medium. The formation of the punctate mineral deposits was confirmed to be hydroxyapatite across all three hydrogel conditions by Raman spectroscopy. Although the growth medium lacked

the phosphate additive, β-glycerophosphate, this medium contains sodium phosphate, which may act as a phosphate source for mineral depositions [49]. These data suggest MC3T3-E1 cells, as they differentiate, facilitate mineral deposition likely through cell-secreted mineralizing proteins combined with available calcium and phosphate ions in the culture medium. In the hydrogels with incorporated hydroxyapatite nanoparticles, these particles may slowly release ions as a result of dissolution [45], which can then serve as an additional source of ions for cell-mediated mineralization. It is also possible that the particles themselves may have served as nucleation sites that led to mineral growth at the surface of the nanoparticles [21]. The ECM also comprised collagen, which was highest in the 1% hydroxyapatite condition. Collagen type I fibrils have been shown to participate in the process of bone mineralization [50] and thus may have contributed to the observed mineralization. The combination of more abundant mineral deposits and higher collagen content suggests that these MMP-sensitive PEG hydrogels when combined with hydroxyapatite nanoparticles create an osteoinductive environment that supports deposition of bone-like ECM molecules by MC3T3-E1 cells in growth medium.

In differentiation medium, similar trends were observed with increasing hydroxyapatite, but the amount of bone-like ECM deposition was much greater. With the highest hydroxyapatite condition, mineral deposition was present throughout the hydrogel construct, which corresponded to a greater spatial deposition of collagen type I. The more elaborate mineral deposits were confirmed to be in large part a result of the nanoparticles themselves serving as nucleation sites for additional mineralization. This was not observed with the 0.1% hydroxyapatite, which may be attributed to the need to be above a critical threshold density of hydroxyapatite nanoparticles for the particles themselves to nucleate mineralization [21]. The more elaborate ECM, especially for collagen, may in part be attributed to increased degradation of the hydrogel, which is evident by increased cell spreading and can only occur as a result of hydrogel degradation [32]. For large ECM molecules, such as collagen, the hydrogel must reach its reverse gelation point in order for these molecules to form an interconnected matrix [51]. Interestingly, the compressive modulus remained fairly constant suggesting that as the cells degrade the hydrogel, deposition of ECM may counteract the loss in modulus by the hydrogel. Additional studies, however, are needed to identify the degree to which the hydrogel is still present. Collectively, these results suggest that osteogenic factors present in the culture medium coupled with the presence of hydroxyapatite nanoparticles significantly enhances osteogenesis and ECM deposition and elaboration; a finding that is likely mediated in part by increased MMP activity as a result of osteogenesis.

Conclusion

This study demonstrates that incorporating hydroxyapatite nanoparticles into a MMP-sensitive PEG hydrogel with RGD cell adhesion ligands creates an osteoinductive environment that enhances osteogenesis of encapsulated MC3T3-E1 pre-osteoblasts. Although the concentration of hydroxyapatite was relatively low, at 0.1 and 1% (w/w), the nanoparticles led to enhanced alkaline phosphatase activity, increased mineral deposition, and higher total collagen contents with increasing hydroxyapatite nanoparticle concentration. Osteogenesis was enhanced without the need to include differentiation factors in the culture medium. However, osteogenic differentiation medium coupled with the

inclusion of hydroxyapatite nanoparticles led to cell-mediated degradation of the hydrogel, cell spreading and the greatest osteogenesis and bone-like ECM deposition. In summary, a biomimetic hydrogel comprised of MMP-sensitive crosslinks, RGD cell adhesion peptides, and 1% (w/w) hydroxyapatite nanoparticles is a promising hydrogel for bone tissue engineering. Future research will need to test this hydrogel in a relevant *in vivo* bone defect model to determine whether the osteoinductive capabilities are sufficient to promote bone growth *in vivo*.

Acknowledgments

Research reported in this publication was supported by the National Institute of Arthritis and Musculoskeletal and Skin Diseases of the National Institutes of Health under Award Number 1R01AR069060. The content is solely the responsibility of the authors and does not necessarily represent the official views of the National Institutes of Health. The authors acknowledge support the Balsells Fellowship to MCC and a Department of Education GAANN fellowship to LSS.

References

1. Alsberg E, Franceschi RT, Mooney DJ. Bone tissue engineering using injectable hydrogels. J Dent Res. 2000; 79:94.
2. Kondiah PJ, Choonara YE, Kondiah PPD, Marimuthu T, Kumar P, du Toit LC, Pillay V. A Review of Injectable Polymeric Hydrogel Systems for Application in Bone Tissue Engineering. Molecules. 2016; 21:1580.
3. Li Y, Rodrigues J, Tomas H. Injectable and biodegradable hydrogels: gelation, biodegradation and biomedical applications. Chem Soc Rev. 2012; 41:2193–221. [PubMed: 22116474]
4. Nicodemus GD, Bryant SJ. Cell Encapsulation in Biodegradable Hydrogels for Tissue Engineering Applications. Tissue Eng Part B. 2008; 14:149–65.
5. Tibbitt MW, Anseth KS. Hydrogels as Extracellular Matrix Mimics for 3D Cell Culture. Biotechnol Bioeng. 2009; 103:655–63. [PubMed: 19472329]
6. Zhu M, Lin S, Sun Y, Feng Q, Li G, Bian L. Hydrogels functionalized with N-cadherin mimetic peptide enhance osteogenesis of hMSCs by emulating the osteogenic niche. Biomaterials. 2016; 77:44–52. [PubMed: 26580785]
7. Kim S, Cui Z-K, Fan J, Fartash A, Aghaloo TL, Lee M. Photocrosslinkable chitosan hydrogels functionalized with the RGD peptide and phosphoserine to enhance osteogenesis. J Mater Chem B. 2016; 4:5289–98. [PubMed: 28044100]
8. Niu Y, Li Q, Xie R, Liu S, Wang R, Xing P, Shi Y, Wang Y, Dong L, Wang C. Modulating the phenotype of host macrophages to enhance osteogenesis in MSC-laden hydrogels: Design of a glucomannan coating material. Biomaterials. 2017; 139:39–55. [PubMed: 28582717]
9. West JL, Hubbell JA. Polymeric biomaterials with degradation sites for proteases involved in cell migration. Macromolecules. 1999; 32:241–4.
10. Lutolf MP, Hubbell JA. Synthetic biomaterials as instructive extracellular microenvironments for morphogenesis in tissue engineering. Nat Biotechnol. 2005; 23:47–55. [PubMed: 15637621]
11. Liu M, Zeng X, Ma C, Yi H, Ali Z, Mou X, Li S, Deng Y, He N. Injectable hydrogels for cartilage and bone tissue engineering. Bone Res. 2017; 5:17014. [PubMed: 28584674]
12. Hersel U, Dahmen C, Kessler H. RGD modified polymers: biomaterials for stimulated cell adhesion and beyond. Biomaterials. 2003; 24:4385–415. [PubMed: 12922151]
13. Gandavarapu NR, Alge DL, Anseth KS. Osteogenic differentiation of human mesenchymal stem cells on alpha5 integrin binding peptide hydrogels is dependent on substrate elasticity. Biomater Sci. 2014; 2:352–61. [PubMed: 24660057]
14. Hamidouche Z, Fromigue O, Ringe J, Haupl T, Vaudin P, Pages JC, Srouji S, Livne E, Marie PJ. Priming integrin alpha 5 promotes human mesenchymal stromal cell osteoblast differentiation and osteogenesis. Proc Natl Acad Sci U S A. 2009; 106:18587–91. [PubMed: 19843692]

15. Nuttelman CR, Tripodi MC, Anseth KS. Synthetic hydrogel niches that promote hMSC viability. Matrix Biol. 2005; 24:208–18. [PubMed: 15896949]
16. Gao G, Yonezawa T, Hubbell K, Dai G, Cui X. Inkjet-bioprinted acrylated peptides and PEG hydrogel with human mesenchymal stem cells promote robust bone and cartilage formation with minimal printhead clogging. Biotechnol J. 2015; 10:1568–77. [PubMed: 25641582]
17. Anderson SB, Lin CC, Kuntzler DV, Anseth KS. The performance of human mesenchymal stem cells encapsulated in cell-degradable polymer-peptide hydrogels. Biomaterials. 2011; 32:3564–74. [PubMed: 21334063]
18. Lutolf MR, Weber FE, Schmoekel HG, Schense JC, Kohler T, Muller R, Hubbell JA. Repair of bone defects using synthetic mimetics of collagenous extracellular matrices. Nat Biotechnol. 2003; 21:513–8. [PubMed: 12704396]
19. Kim J, Kim IS, Cho TH, Kim HC, Yoon SJ, Choi J, Park Y, Sun K, Hwang SJ. In vivo evaluation of MMP sensitive high-molecular weight HA-based hydrogels for bone tissue engineering. J Biomed Mater Res A. 2010; 95:673–81. [PubMed: 20725983]
20. LeGeros RZ. Calcium Phosphate-Based Osteoinductive Materials. Chem Rev. 2008; 108:4742–53. [PubMed: 19006399]
21. Nejadnik MR, Mikos AG, Jansen JA, Leeuwenburgh SCG. Facilitating the mineralization of oligo(poly(ethylene glycol) fumarate) hydrogel by incorporation of hydroxyapatite nanoparticles. J Biomed Mater Res A. 2012; 100A:1316–23.
22. Leeuwenburgh SCG, Jansen JA, Mikos AG. Functionalization of oligo(poly(ethylene glycol)fumarate) hydrogels with finely dispersed calcium phosphate nanocrystals for bone-substituting purposes. J Biomater Sci-Polym Ed. 2007; 18:1547–64. [PubMed: 17988519]
23. Nijhuis AWG, Takemoto S, Nejadnik MR, Li Y, Yang X, Ossipov DA, Hilborn J, Mikos AG, Yoshinari M, Jansen JA, Leeuwenburgh SCG. Rapid Screening of Mineralization Capacity of Biomaterials by Means of Quantification of Enzymatically Deposited Calcium Phosphate. Tissue Eng Part C-Methods. 2014; 20:838–50. [PubMed: 24650236]
24. Juhasz JA, Best SM, Bonfield W. Preparation of novel bioactive nano-calcium phosphate-hydrogel composites. Sci Technol Adv Mater. 2010; 11:014103. [PubMed: 27877318]
25. Dhivya S, Saravanan S, Sastry TP, Selvamurugan N. Nanohydroxyapatite-reinforced chitosan composite hydrogel for bone tissue repair in vitro and in vivo. J Nanobiotechnology. 2015; 13:40. [PubMed: 26065678]
26. Wenz A, Borchers K, Tovar GEM, Kluger PJ. Bone matrix production in hydroxyapatite-modified hydrogels suitable for bone bioprinting. Biofabrication. 2017; 9:044103. [PubMed: 28990579]
27. Lin GY, Tarasevich B. Photopolymerized hydrogel composites from poly(ethylene glycol) and hydroxyapatite for controlled protein delivery in vitro. J Appl Polym Sci. 2013; 128:3534–9.
28. Killion JA, Geever LM, Devine DM, Higginbotham CL. Fabrication and invitro biological evaluation of photopolymerisable hydroxyapatite hydrogel composites for bone regeneration. J Biomater Appl. 2014; 28:1274–83. [PubMed: 24114559]
29. Gaharwar AK, Dammu SA, Canter JM, Wu C-J, Schmidt G. Highly Extensible, Tough, and Elastomeric Nanocomposite Hydrogels from Poly(ethylene glycol) and Hydroxyapatite Nanoparticles. Biomacromolecules. 2011; 12:1641–50. [PubMed: 21413708]
30. Supova M. Problem of hydroxyapatite dispersion in polymer matrices: a review. J Mater Sci-Mater Med. 2009; 20:1201–13. [PubMed: 19225871]
31. Fairbanks BD, Schwartz MP, Halevi AE, Nuttelman CR, Bowman CN, Anseth KS. A Versatile Synthetic Extracellular Matrix Mimic via Thiol-Norbornene Photopolymerization. Adv Mater. 2009; 21:5005–10. [PubMed: 25377720]
32. Amer LD, Bryant SJ. The In Vitro and In Vivo Response to MMP-Sensitive Poly(Ethylene Glycol) Hydrogels. Ann Biomed Eng. 2016; 44:1959–69. [PubMed: 27080375]
33. Quarles L, Yohay D, Lever L, Caton R, WENSTRUP R. Distinct proliferative and differentiated stages of murine MC3T3-31 cells in culture - an inv itro model of osteoblast development. J Bone Miner Res. 1992; 7:683–92. [PubMed: 1414487]
34. Di Cio S, Gautrot JE. Cell sensing of physical properties at the nanoscale: Mechanisms and control of cell adhesion and phenotype. Acta Biomater. 2016; 30:26–48. [PubMed: 26596568]

35. Guvendiren M, Burdick JA. Engineering synthetic hydrogel microenvironments to instruct stem cells. Curr Opin Biotechnol. 2013; 24:841–6. [PubMed: 23545441]
36. Huebsch N, Arany PR, Mao AS, Shvartsman D, Ali OA, Bencherif SA, Rivera-Feliciano J, Mooney DJ. Harnessing traction-mediated manipulation of the cell/matrix interface to control stem-cell fate. Nat Mater. 2010; 9:518–26. [PubMed: 20418863]
37. Khetan S, Guvendiren M, Legant WR, Cohen DM, Chen CS, Burdick JA. Degradation-mediated cellular traction directs stem cell fate in covalently crosslinked three-dimensional hydrogels. Nat Mater. 2013; 12:458–65. [PubMed: 23524375]
38. Karsdal MA, Andersen TA, Bonewald L, Christiansen C. Matrix metalloproteinases (MMPs) safeguard osteoblasts from apoptosis during transdifferentiation into osteocytes: MT1-MMP maintains osteocyte viability. DNA Cell Biol. 2004; 23:155–65. [PubMed: 15068585]
39. Hakki SS, Bozkurt SB, Hakki EE, Korkusuz P, Purali N, Koc N, Timucin M, Ozturk A, Korkusuz F. Osteogenic differentiation of MC3T3-E1 cells on different titanium surfaces. Biomed Mater Bristol Engl. 2012; 7:045006.
40. Mullen CA, Vaughan TJ, Voisin MC, Brennan MA, Layrolle P, McNamara LM. Cell morphology and focal adhesion location alters internal cell stress. J R Soc Interface. 2014:11.
41. Lin LW, Chow L, Leng Y. Study of hydroxyapatite osteoinductivity with an osteogenic differentiation of mesenchymal stem cells. J Biomed Mater Res A. 2009; 89A:326–35.
42. Wei GB, Ma PX. Structure and properties of nano-hydroxyapatite/polymer composite scaffolds for bone tissue engineering. Biomaterials. 2004; 25:4749–57. [PubMed: 15120521]
43. Bose S, Tarafder S. Calcium phosphate ceramic systems in growth factor and drug delivery for bone tissue engineering: A review. Acta Biomater. 2012; 8:1401–21. [PubMed: 22127225]
44. Liu Y, Wang G, Cai Y, Ji H, Zhou G, Zhao X, Tang R, Zhang M. In vitro effects of nanophase hydroxyapatite particles on proliferation and osteogenic differentiation of bone marrow-derived mesenchymal stem cells. J Biomed Mater Res A. 2009; 90A:1083–91.
45. Porter A, Patel N, Brooks R, Best S, Rushton N, Bonfield W. Effect of carbonate substitution on the ultrastructural characteristics of hydroxyapatite implants. J Mater Sci Mater Med. 2005; 16:899–907. [PubMed: 16167098]
46. Sun S, Liu Y, Lipsky S, Cho M. Physical manipulation of calcium oscillations facilitates osteodifferentiation of human mesenchymal stem cells. FASEB J Off Publ Fed Am Soc Exp Biol. 2007; 21:1472–80.
47. Bryant, SJ., Anseth, KS. Photopolymerization of hydrogel scaffolds. CRC; 2005.
48. Chen G, Deng C, Li Y-P. TGF-β and BMP Signaling in Osteoblast Differentiation and Bone Formation. Int J Biol Sci. 2012; 8:272–88. [PubMed: 22298955]
49. Pham Minh D, Lyczko N, Sebei H, Nzihou A, Sharrock P. Synthesis of calcium hydroxyapatite from calcium carbonate and different orthophosphate sources: A comparative study. Mater Sci Eng B. 2012; 177:1080–9.
50. Nudelman F, Pieterse K, George A, Bomans PHH, Friedrich H, Brylka LJ, Hilbers PAJ, de With G, Sommerdijk NAJM. The role of collagen in bone apatite formation in the presence of hydroxyapatite nucleation inhibitors. Nat Mater. 2010; 9:1004–9. [PubMed: 20972429]
51. Bryant SJ, Vernerey FJ. Programmable Hydrogels for Cell Encapsulation and Neo-Tissue Growth to Enable Personalized Tissue Engineering. Adv Healthc Mater. 2018:7.

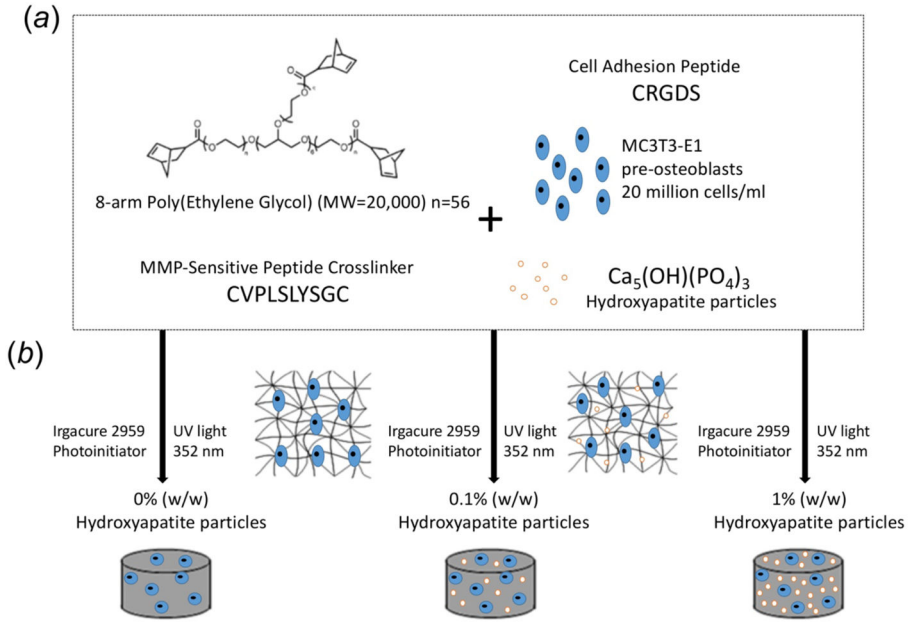

Figure 1.

Schematic illustrating the experimental study design. In (*a*) hydrogel precursors, MC3T3-E1 pre-osteoblasts, and hydroxyapatite nanoparticles are mixed into a solution. In (*b*) MMP-sensitive PEG hydrogels containing tethered RGD cell adhesion ligands, embedded hydroxyapatite nanoparticles, and encapsulated MC3T3-E1 cells are formed via a thiol-norbornene reaction in the presence of light and a photoinitiator. Three experimental groups are investigated in this study with varying concentrations (0, 0.1, and 1% (w/w)) of hydroxyapatite nanoparticles.

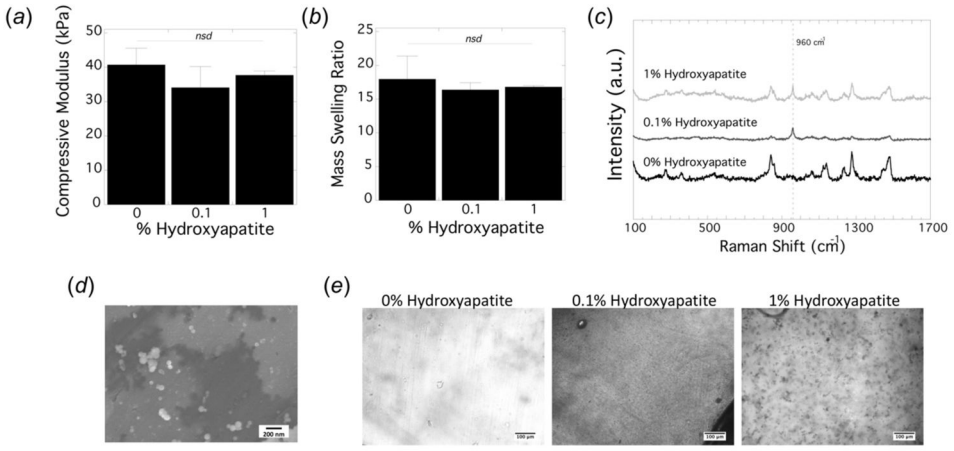

Figure 2.

Characterization of acellular hydrogels with increasing concentration of hydroxyapatite nanoparticles: (*a*) compressive modulus, (*b*) mass swelling ratio, and (*c*) and Raman spectroscopy confirming the presence of the characteristic hydroxyapatite peak at 960 cm^{-1} in the hydrogels with hydroxyapatite nanoparticles, but absent in the hydrogels with not hydroxyapatite nanoparticles. Characterization of hydroxyapatite nanoparticles: (*d*) scanning electron microscopy of particles prior to encapsulating in the hydrogels and (*e*) bright field images showing distribution of nanoparticles within acellular hydrogels. Data are reported as mean with standard deviation as error bars in (*a*) and (*b*); *nsd*=not statistically different (n=3).

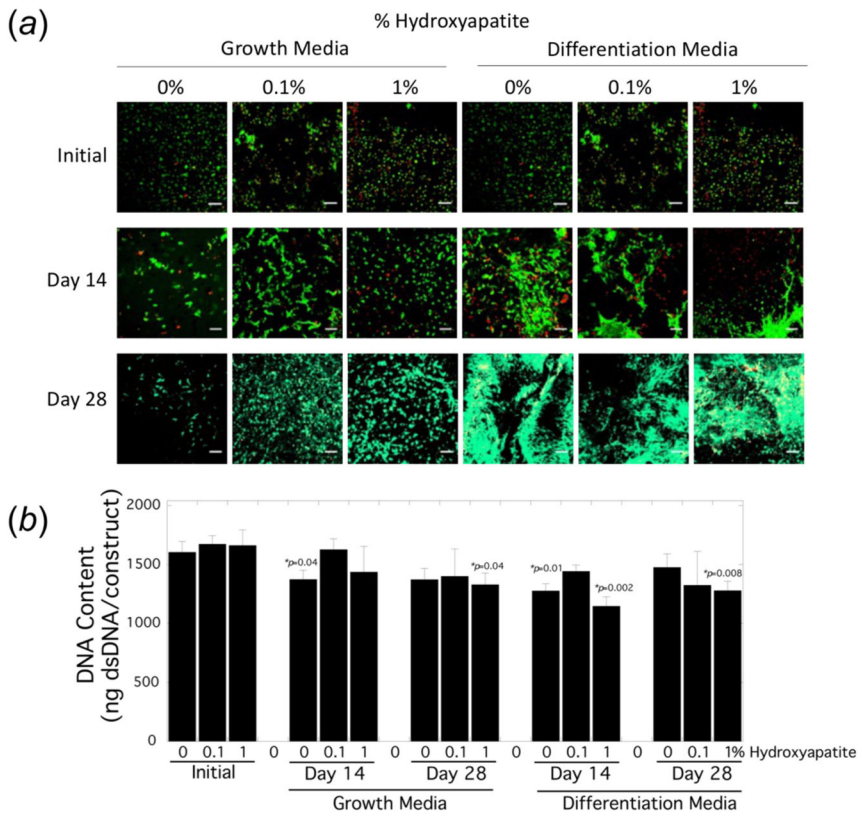

Figure 3.

Characterization of acellular hydrogels with increasing concentration of hydroxyapatite nanoparticles: (*a*) compressive modulus, (*b*) mass swelling ratio, and (*c*) and Raman spectroscopy confirming the presence of the characteristic hydroxyapatite peak at 960 cm^{-1} in the hydrogels with hydroxyapatite nanoparticles, but absent in the hydrogels with not hydroxyapatite nanoparticles. Data are reported as mean with standard deviation as error bars in (*a*) and (*b*); *nsd*=not statistically different (n=3). Cellular viability, morphology, and content for each experimental group with varying concentration of hydroxyapatite nanoparticle concentration, culture medium (growth media or differentiation media) and culture time. (*a*) Representative confocal microscopy images of viable (green) and dead (red) MC3T3-E1 cells encapsulated in the mimetic hydrogels initially (i.e., 24 hours post-encapsulation) and at days 14 and 28. Scale bar is 100 μm. (*b*) DNA (double stranded, ds) content per hydrogel construct as a measure of cellular content. Data are reported as mean with standard deviation as error bars for n=3. *P*-values indicate significant difference from the initial time point for the corresponding hydroxyapatite concentration and culture medium.

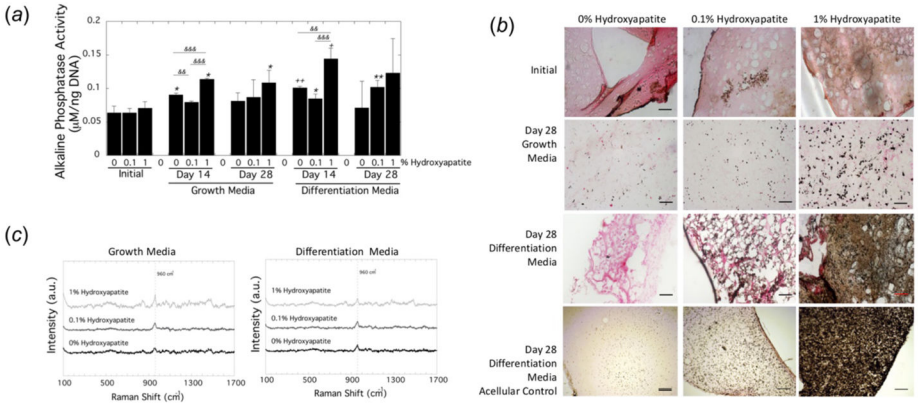

Figure 4.

Characterization of hydrogels associated with mineral deposition for each experimental group with varying concentration of hydroxyapatite nanoparticle concentration, culture medium (growth media or differentiation media) and culture time. In (a), alkaline phosphatase activity normalized to DNA content for encapsulated MC3T3-E1 cells as a measure of osteogenic differentiation. Data are reported as mean with standard deviation as error bars for n=3. *P*-values denoted by * indicate significant difference from the initial time point for the corresponding hydroxyapatite concentration and culture medium (* $p<0.05$; ** $p<0.01$; *** $p<0.001$). *P*-values denoted by + indicate significant difference from the growth media condition for the corresponding hydroxyapatite concentration and time point (+ $p<0.05$; ++ $p<0.01$; +++ $p<0.001$). *P*-values denoted by & indicate significant differences between the two corresponding data points (& $p<0.05$; && $p<0.01$; &&& $p<0.001$). In (*b*), representative microscopy images of sections stained by von Kossa for mineral deposits in cellular hydrogels containing encapsulated MC3T3-E1 cells initial and at day 28 in growth and differentiation media and in acellular hydrogels at day 28 in differentiation medium. Mineral stains black and cell nuclei stain pink. Scale bar is 100 μm. In (*c*) representative Raman spectra (n=3) from regions of the hydrogel sections that stained positive for mineral by von Kossa at 28 days in growth medium (*left*) and differentiation medium (*right*). The characteristic hydroxyapatite peak at 960 cm^{-1} is denoted on the plots.

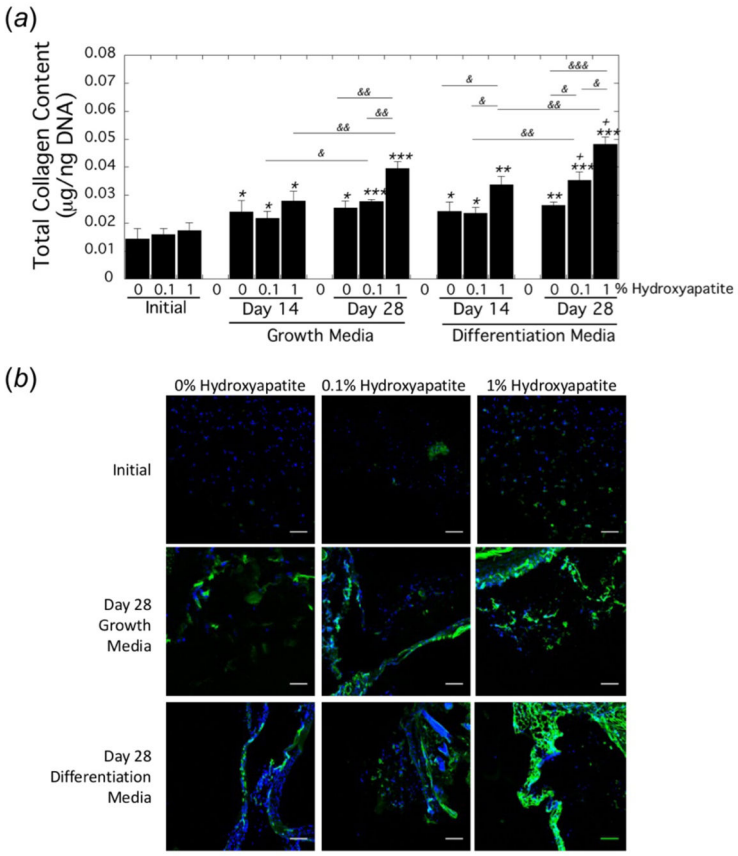

Figure 5.

Characterization of hydrogels associated with collagen deposition for each experimental group with varying concentration of hydroxyapatite nanoparticle concentration, culture medium (growth media or differentiation media) and culture time. In (a), total collagen content normalized to DNA content for encapsulated MC3T3-E1 cells. Data are reported as mean with standard deviation as error bars for n=3. *P*-values denoted by * indicate significant difference from the initial time point for the corresponding hydroxyapatite concentration and culture medium (* $p<0.05$; ** $p<0.01$; *** $p<0.001$). *P*-values denoted by $^{+}$ indicate significant difference from the growth media condition for the corresponding hydroxyapatite concentration and time point ($^{+}$ $p<0.05$; $^{++}$ $p<0.01$; $^{+++}$ $p<0.001$). *P*-values denoted by $^{\&}$ indicate significant differences between the two corresponding data points ($^{\&}$ $p<0.05$; $^{\&\&}$ $p<0.01$; $^{\&\&\&}$ $p<0.001$). In (*b*), representative confocal microscopy images of sections stained for collagen type I by encapsulated MC3T3-E1 cells. Collagen type I stains green and cell nuclei stain blue. Scale bar is 50 µm.

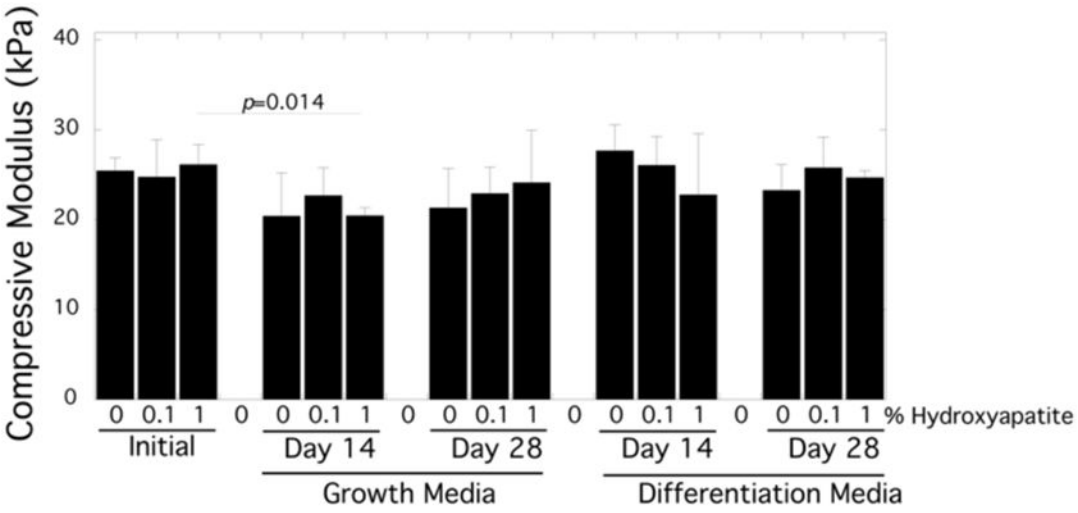

Figure 6.

Characterization of the compressive modulus of hydrogels for each experimental group with varying concentration of hydroxyapatite nanoparticle concentration, culture medium (growth media or differentiation media) and culture time. Data are reported as mean with standard deviation as error bars for n=3. *P*-values indicate significant differences between the two corresponding data.